Design and Optimization of a Micro Heat Sink for Concentrating Photovoltaic/Thermal (CPVT) Systems

Ioannis K. KARATHANASSIS [1, 2, *], Elias PAPANICOLAOU [1], Vassilios BELESSIOTIS [1], Georgios C. BERGELES [2]

* Corresponding author: Tel.: ++30 210 6503815; Fax: ++30 210 6544592;
Email: ikarathanassis@ipta.demokritos.gr
1 Solar & other Energy Systems Laboratory, Institute of Nuclear Technology & Radiation Protection, National Centre for Scientific Research DEMOKRITOS, Greece, Email: sollab@ipta.demokritos.gr
2 Laboratory of Innovative Environmental Technologies, School of Mechanical Engineering, National Technical University of Athens, Greece, Email: bergeles@fluid.mech.ntua.gr

Abstract An optimization methodology for a microchannel heat sink suitable for the cooling of a parabolic trough CPVT system is presented in this study. Two different microchannel configurations are considered, Fixed (FWμ) and stepwise Variable-Width (VWμ) microchannels respectively. The performance evaluation criteria comprise the thermal resistance of the heat sink and the cooling medium pressure drop through the heat sink. Initially, the effect of the geometric parameters on the heat sink thermal and hydrodynamic performance is investigated using a thermal resistance model in order to save computational time. The results of the 1-D model enable the construction of surrogate functions for the thermal resistance and the pressure drop of the heat sink, which are considered as the objective functions for the multiobjective optimization process that leads to the optimal geometric parameters. In a second step, a 3-D numerical model of fluid flow and conjugate heat transfer in the optimized FWμ heat sink is developed in order to investigate in detail the flow and thermal phenomena. The overall analysis demonstrates that microchannel heat sinks achieve very low values of thermal resistance and that the use of variable-width channels can significantly reduce the pressure drop of the cooling fluid. Furthermore, it is proven that the 1-D model is capable of providing a good estimate of the behavior of the heat sink.

Keywords: CPVT, Micro Heat Sink, Conjugate Heat Transfer, Response surfaces, Genetic algorithms, Multiobjective optimization

1. Introduction

The use of microchannel heat sinks is a common practice for the cooling of Very Large Scale Integrated (VLSI) circuits, where the dissipation of extremely high heat fluxes is necessary. Tuckerman and Pease (1981) were the first to demonstrate, that using channels with a hydraulic diameter in the microscale region, can make the dissipation of heat fluxes as high as 790 W/cm^2 possible. A number of either analytical or numerical methods has been reported by various researchers (Goldberg, 1984; Knight, 1991; Mueller, 2002; Liu, 2003; Husain, 2008) in order to determine the optimum geometrical parameters that maximize the performance of a microchannel heat sink

In a similar manner, Concentrating Photo-Voltaic Thermal Systems (CPVT) use optical devices to concentrate solar radiation onto a very small area and therefore the presence of a high heat flux on the solar cell module renders the use of a microchannel heat sink necessary, in order to extract the surplus heat and keep the operating temperature of the solar cell module low. In the present work, a microchannel heat sink is utilized in a parabolic trough CPVT system, serving the dual purpose of cooling the solar module and extracting useful thermal energy.

2. Heat Sink Configurations

The microchannel heat sink is bonded to the backside of a solar cell module, Fig. 1, on the front side of which, a constant flux of concentrated solar radiation is incident. A

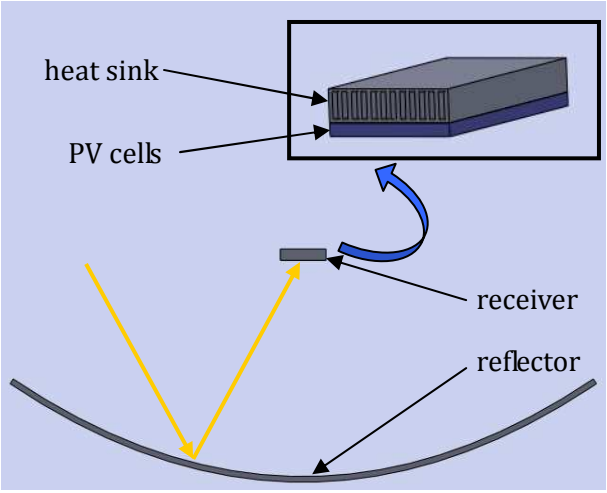

Fig. 1 Schematic of the CPVT system.

percentage of the incoming irradiation, in the order of 15-20%, is absorbed by the PV module and directly converted to electricity. The remaining energy is converted into heat to be extracted by the heat sink, which is made of aluminum, due to the high thermal conductivity of the material (k_{al}=*237W/mK*). The total area of the microchannel heat sink, corresponding to the area of the CPVT system receiver, is 0.5 x 0.06m^2. The parabolic reflector aperture is equal to 1 m^2 so that a constant flux of 33kW/m^2 is incident on the PV surface. Water was chosen as the cooling medium with a total volumetric flow rate of 30ml/s, which is sufficient for a system producing hot water at 60^{o}C for domestic use. The cooling fluid, after entering the heat sink through an inlet nozzle, branches into parallel channels, the number N of which is determined by the channel width W_{ch} and the wall thickness W_w as follows:

$$N = \frac{W_{hs} - aW_{ch}}{(a+1)W_{ch}}, \text{ where } a = \frac{W_w}{W_{ch}} \qquad (1)$$

Thus, the flow inside each microchannel is characterized by the Reynolds number defined as:

$$Re = \frac{\left(\dot{V}_{tot}/N\right)D_h}{A_{ch,cs}\nu} \qquad (2)$$

3. 1-D Analysis

3.1 Fixed-width microchannels (FWμ)

The thermal and hydrodynamic performance of the microchannel heat sink was predicted by means of a one-dimensional thermal resistance model. Initially, in order to evaluate the thermal performance of the heat sink, the equivalent thermal resistance model was employed (Kraus & Bar-Cohen, 1983). The total thermal resistance of the heat sink is:

$$R_{tot} = R_{cond} + R_{cal} + R_{conv} \qquad (3)$$

The conductive and caloric thermal resistances are:

$$R_{cond} = \frac{t_s}{k_s A} \qquad R_{cal} = \frac{1}{\rho Q_{tot} c_p} \qquad (4)$$

As the conductive thermal resistance is dependent only on the thickness of the substrate, it will not be included in the following analysis. The convective thermal resistance is given by:

$$R_{conv} = \frac{1}{hA} = \frac{1}{h\left[N\left(2\eta_{fin}H_{ch} + W_{ch}\right)L\right]} = \frac{T_{w,\max} - T_{f,i}}{Q} \qquad (5)$$

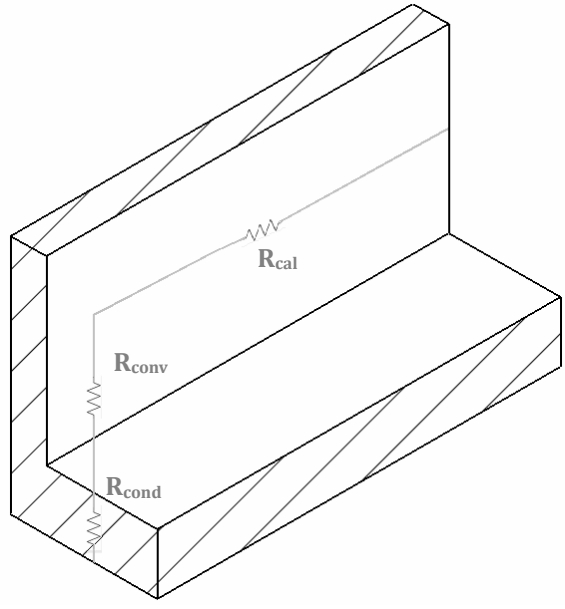

Fig. 2 Thermal resistance model for a FWμ heat sink.

The overall heat transfer coefficient is considered uniform over the channel base and vertical walls and since the flow lies almost entirely in the fully developed region, the corresponding Nusselt number value, is taken constant for a given geometry and can be easily obtained from analytical correlations or tabulated values (Shah and London, 1978).

The side walls of the microchannels are thought of as fins with efficiency:

$$\eta = \frac{tanh(mH_{ch})}{mH_{ch}} \quad \text{where} \quad m = \sqrt{\frac{2h}{k_s W_w}} \tag{6}$$

The hydrodynamic performance of the heat sink is described by the total pressure drop of the cooling fluid:

$$\Delta p_{tot} = \Delta p_c + \Delta p_d + \Delta p_{fd} + \Delta p_e \tag{7}$$

The four terms on the right-hand side of Eq. (7) refer to the pressure drop in the entrance, the developing flow region, the fully developed region and the exit of the microchannel respectively, where the last term is negligibly small. The pressure drop due to contraction can be calculated from an analytical correlation given by Blevins (1984), whereas the pressure drop in the developing and the fully developed region is expressed by a relation of the general form:

$$\Delta p = \frac{2\rho f L u_m^2}{D_h} \tag{8}$$

where L is the length of the entrance region (or development length), correlations for which are given by Shah and Bhatti (1987), or the length of the fully developed region respectively, and f should be substituted by the apparent Fanning friction factor in the developing region (Shah, 1978) or accordingly by the Fanning friction factor for fully developed flow (Shah and London, 1978; Lee, 2007).

3.2 Variable-width microchannels (VWμ)

The concept of the stepwise variable-width (VW) microchannel heat sink (Fig. 3a) is based on two basic remarks. On one hand, by reducing the channel width, while maintaining the height constant, the Nusselt number increases (Shah and London, 1978) and so does also the total heat transfer coefficient, which is further enhanced by the reduction of the hydraulic diameter. On the other hand, upon reduction of the hydraulic diameter the Fanning friction factor and thus the pressure drop also, increases.

In the case of a microchannel heat sink of constant hydraulic diameter which receives a uniform heat flux, the bottom wall and the bulk fluid temperature both increase in a similar linear manner, when the flow becomes fully developed (Incropera and Dewitt, 1996). The only option for enhancing the temperature uniformity of the bottom wall is therefore to gradually increase the heat transfer coefficient along the direction of the flow by adding more heat transfer surfaces (Barrau et al., 2010). Additionally, using wider channels in the first section of the heat sink, where the bulk fluid temperature is low, decreases the overall pressure drop.

In order for such a heat sink to be structurally feasible, the width of the channel along consecutive sections must be decreased in the following manner:

$$W_{ch,downstream} = \frac{W_{ch,upstream}}{2} - \frac{W_w}{2} \tag{9}$$

The total thermal resistance of the VWμ heat sink can be determined by Eq. (3), if a mean convective resistance is defined as for the case of parallel resistances:

$$\frac{1}{R_{conv,tot}} = \sum_{i=1}^{Ns} \frac{1}{R_{conv,i}} = \sum_{i=1}^{Ns} \frac{1}{h_i A_i} \tag{10}$$

where N_s is the number of sections, taken equal to three in the present analysis. Eq. (10) results if we consider the equivalent thermal resistance circuit, Fig. 3b, where the parallel resistances represent the equal-length sections of different hydraulic diameters. The total pressure drop can be obtained by adding the pressure drop values along each section as derived by Eq. (7). It should be noted that,

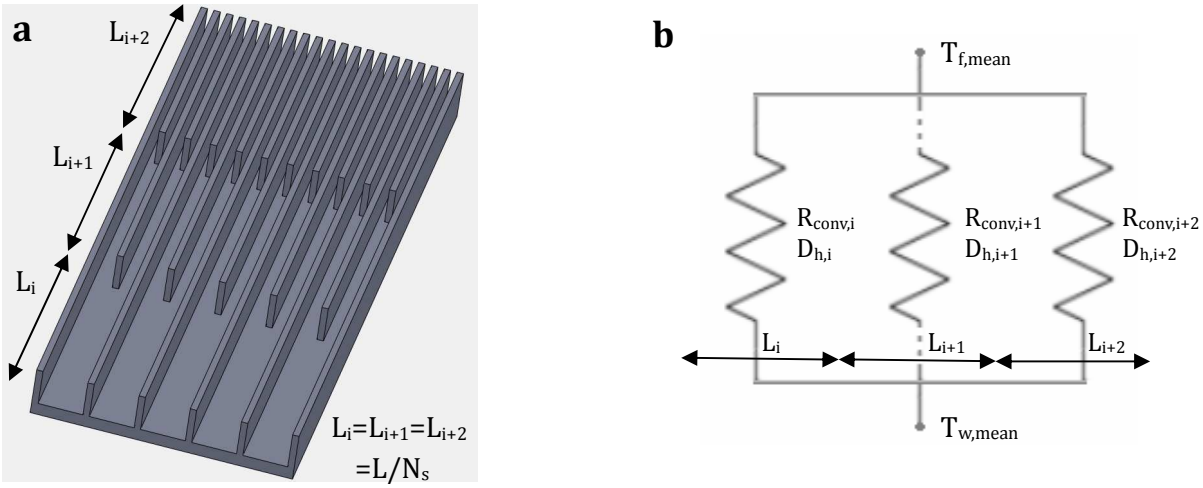

Fig. 3 VWμ heat sink: (a) Layout and (b) equivalent thermal resistance network.

depending on the hydraulic diameter of the channels, the volumetric flow rate and the length of each section, the flow could be developing or fully developed and therefore the proper values for the Nusselt number and the Fanning friction factor should be selected.

4. Optimization

4.1 Objective functions and design variables determination

The thermal and hydraulic behavior of the heat sink can be fully described by the sum of the convective and the caloric thermal resistance, Eq. (4), and the required pumping power, which is defined as:

$$P_{pump} = \dot{V}_{tot} \Delta p \tag{11}$$

These two quantities are selected as the objective functions for the optimization process.

The total width and length of the microchannel heat sink are fixed and therefore the design parameters which determine the heat sink performance and can be included in the optimization process are the channel width and aspect ratio (H_{ch}/W_{ch}), along with the fin thickness. It is evident from the analytical correlations for the thermal resistance and pressure drop that an increase in the channel aspect ratio has a beneficial impact on both the objective functions, due to the increase of the available heat transfer area and the deceleration of the flow. Therefore, the height is fixed at the maximum structurally possible. Consequently, two independent design variables are selected for optimization, namely the microchannel width W_{ch} and the fin thickness W_w. For the VWμ heat sink in particular, the fin thickness must be maintained constant and as small as structurally possible. This is because the ratio a, Eq. (1), can obtain values much higher than unity, as the channel width decreases in each section, which is undesirable. Consequently, the only design variable that can be altered is the width of the channel of the initial section $W_{ch,init}$.

4.2 Surrogate functions

A pair of design variables (W_{ch}, W_w) produces an output value of both the objective functions. The total of these response values defines a surface which lays above the plane defined by the design variables (Jaluria, 2009) in the three dimensional space. The response values can be adequately approximated by surrogate functions of the type $z = f(x,y)$. A third order polynomial was chosen to approximate the thermal resistance response:

$$\begin{aligned} R_{th}(W_{ch},W_w) = {} & p_{00} + p_{10}W_{ch} + p_{01}W_w + p_{20}W_{ch}^2 \\ & + p_{11}W_{ch}W_w + p_{02}W_w^2 + p_{30}W_{ch}^3 \\ & + p_{21}W_{ch}^2W_w + p_{12}W_{ch}W_w^2 + p_{03}W_w^3 \end{aligned} \tag{12a}$$

Similarly, a power function was selected to approximate the pumping power response, considering the decaying trend that it exhibits:

$$P_{pump}(W_{ch},W_w) = b_1 \cdot W_{ch}^{b_2} \cdot W_w^{b_3} \qquad (12b)$$

Referring to the VWμ microchannels, single-variable surrogate functions are used, as the ratio of the fin thickness to the initial channel width is kept constant to 0.2. Hence, the surrogate functions reduce to the forms:

$$R_{th}(W_{ch,init}) = r_0 + r_1 W_{ch,init} \qquad (13a)$$

$$P_{punp}(W_{ch,init}) = c_1 W_{ch,init}^{c_2} \qquad (13b)$$

4.3 Multi-objective optimization using genetic algorithms

The heat sink optimization constitutes a multiobjective optimization problem, which can be mathematically formulated as follows:

$$\begin{aligned} &min\ \vec{f}(\vec{x}) = [f_1(\vec{x}), f_2(\vec{x}),..., f_i(\vec{x})] \\ &subject\ to\ \vec{g}(\vec{x}) \le 0\ \ and\ \ \vec{h}(\vec{x}) = 0 \end{aligned} \qquad (14)$$

where $\vec{x}$ is the vector that contains the design variables and $\vec{f}(\vec{x}), \vec{g}(\vec{x}), \vec{h}(\vec{x})$ are the vector functions that contain the objective, equality and inequality constraints functions respectively. The multiobjective optimization process converges to a set of non-dominated solutions, called the Pareto front (Deb, 2001).

In order to locate the Pareto front, the genetic algorithm was used, which is a method that uses the rules of biological evolution to solve optimization problems. The algorithm commences by creating a random initial population of design variable vectors, or *individuals*. The individuals are assigned a fitness score according to the value of the fitness function (objective function) that they produce. At each step of the algorithm, a new population, or generation, is created by the members of the current population in a semi-stochastic way, in order for the individual with the best fitness score to prevail after a successive number of generations (Mathworks, 2004). An individual A ($\vec{x}$) is characterized as a non-dominated solution when there is no other individual B, which achieves a better fitness for a single objective ($f_i(\vec{x})$) without deteriorating the other objectives (Hilbert et al., 2006; Ndao et al., 2009).

5. Optimization Results

5.1 Validation

The results of the thermal resistance model for the heat transfer and the pressure drop correlations were compared against the experimental values published by Tuckerman and Pease, who investigated the performance of a silicon (k_{Si}=*148 W/mK*) microchannel heat sink of total dimensions (1 cm) x (1 cm), cooled by water with an initial temperature of 296 K. According to Table 1, the experimental values agree well with the analytically predicted ones. The small discrepancy in the pressure drop values is due to the fact that the analytical model does not account for the pressure loss of the coolant in the inlet-outlet manifold that was used during the experiments, as reported by Tuckerman and Pease (1981)

5.2 Optimal solutions

The design variables for the optimization of the present FWμ and VWμ heat sink configurations were allowed to vary within the following ranges:

$$\begin{aligned} &100\mu m \le W_{ch} \le 500\mu m \\ &100\mu m \le W_w \le 500\mu m \\ &1000\mu m \le W_{ch,init} \le 5000\mu m \end{aligned} \qquad (15)$$

Table 2

Validation of the analytical model.

					R_{th} (^oC/W)		Δp (Pa)	
W_{ch} (μm)	W_w (μm)	H (μm)	q' (W/cm^2)	$\dot{V}_{tot}$ (mL/s)	Experimental	1-D model	Experimental	1-D model
56	44	320	181	4.7	0.110	0.110	103421	92620

where $W_{ch,init}$ refers to the channel width of the initial section of a three-section VWμ heat sink that was selected for the optimization process. The channel height is chosen to be six times the channel width in the FWμ heat sink and two times the initial channel width in the VWμ heat sink. The responses of the 1-D models showed clearly the conflicting nature of the two objective functions as an increase in the thermal resistance leads to a decrease of the pumping power required. Fig.4 illustrates the variation of the objective functions for the FWμ heat sink. The three-section VWμ heat sink exhibits the same behavior, but in the two dimensional space, as the fin width is considered a constraint. Subsequently, appropriate fitting functions were constructed in order to surrogate the analytical values. The surrogates for the objective functions of both heat sink configurations use the coefficients illustrated in Table 2. The quality of the fitting is confirmed by the R^2_{adj} value, which is above 0.99 for all the surrogate functions.

The multiobjective optimization problem was solved using Matlab's multiobjective genetic algorithm. An initial population of 200 individuals evolved for 500 generations, with a crossover probability of 0.8 and a migration probability of 0.2, until a final set of optimal solutions was reached. The Pareto front of non inferior solutions for the two heat sink configurations is illustrated in Fig. 5. The vast majority of optimal solutions for the FWμ heat

Table 2
Coefficients of the surrogate functions.

	FWμ				VWμ
p_{00}	0.008018	p_{30}	1.66E+05	r_0	0.1711
p_{10}	2.033	p_{21}	2.28E+06	r_1	0.008
p_{01}	0.7274	p_{12}	5.79E+06	c_1	4.00E-09
p_{20}	1567	p_{03}	3.84E+06	c_2	-2.9822
p_{11}	-3758	b_1	1.47E-10		
p_{02}	2819	b_2	-3.484		
		b_3	0.675		

sink is shifted towards channels with small hydraulic diameter and thin walls resulting in a configuration with low thermal resistance and high pressure drop.

A similar pattern, regarding the channel width, is also followed by the optimal solutions of the VWμ heat sink. As depicted in Fig. 5b, the utilization of microchannels only in the last part of the heat sink reduces the pressure drop and furthermore, it does not deteriorate the total thermal performance of the heat sink, due to the high microchannel aspect ratio (*AR=20*) in the part of the heat sink where the cooling fluid has a high temperature.

6. 3-D Flow and Heat Transfer Model

In a second stage of this work, the optimal geometrical parameters of the FWμ heat sink were used in order to develop a three dimensional numerical model. The model was

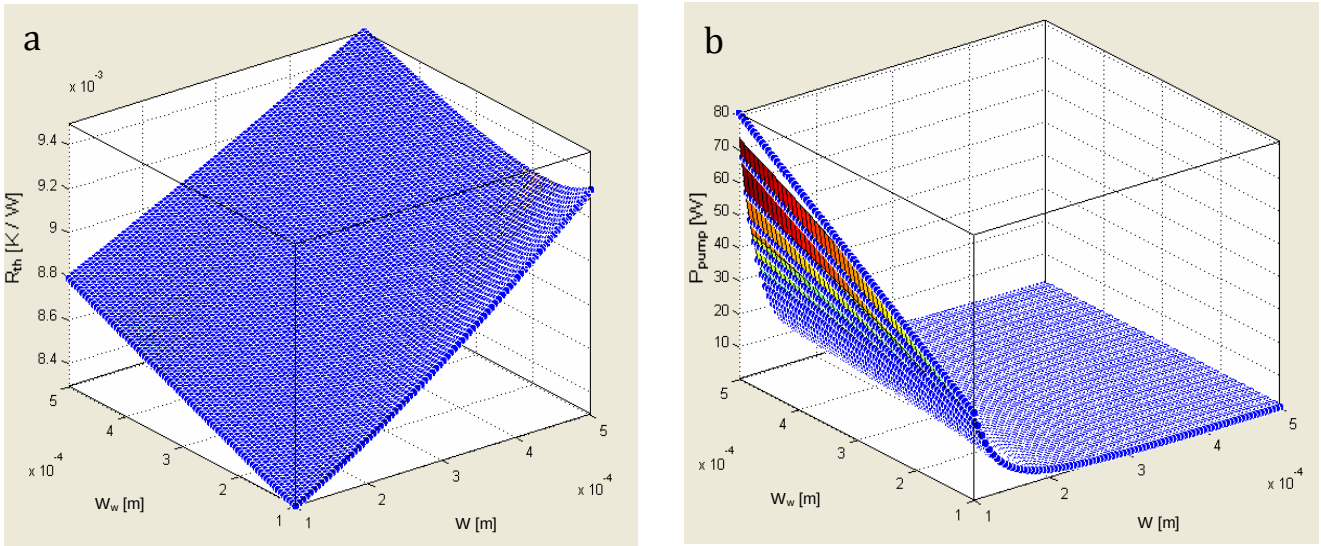

Fig. 4 Response surfaces (a) for the thermal resistance and (b) for the pressure drop of the FWμ heat sink.

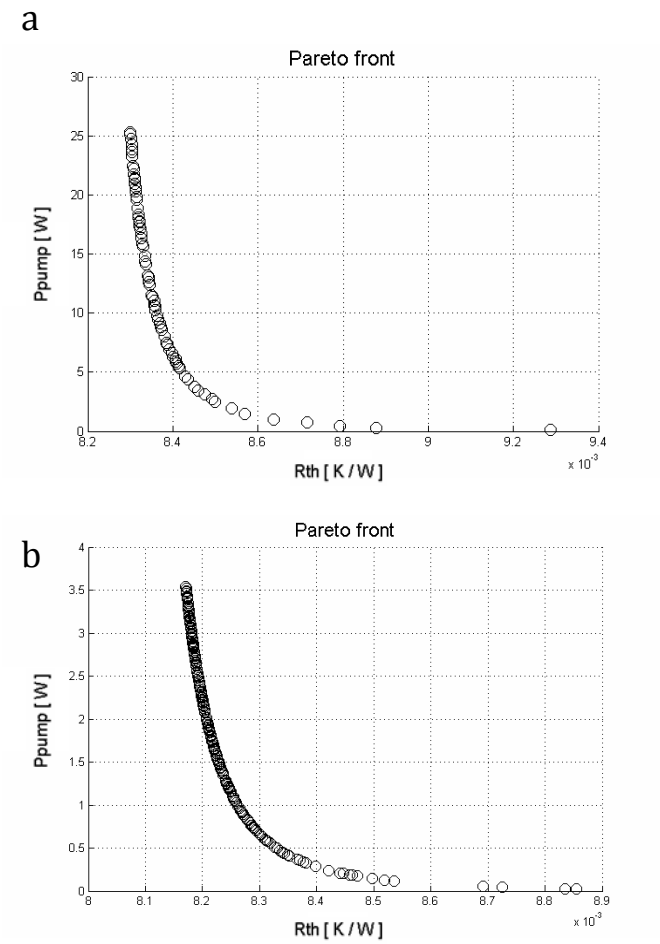

Fig. 5 Pareto front of non dominated solutions (a) for the FWμ heat sink and (b) for the VWμ heat sink.

constructed under the assumptions of steady state, incompressible, single phase and laminar flow. The latter assumption is reasonable considering that for the selected volumetric flow rate and geometrical parameters, the Reynolds number doesn't exceed the value of 320. Moreover, the thermophysical properties of both the fluid and the solid are constant. Based on these assumptions, the governing equations of flow and energy become:

$$\text{(continuity)} \quad \nabla \cdot \left(\rho \vec{V}\right) = 0$$

$$\text{(momentum)} \quad \vec{V} \cdot \nabla\left(\rho \vec{V}\right) = -\nabla p + \nabla\left(\mu \nabla \vec{V}\right) + \Delta\rho \vec{g}$$

$$\text{(energy fluid)} \quad \vec{V} \cdot \nabla\left(\rho c_p T\right) = \nabla\left(k_f \nabla T\right) \qquad (16)$$

$$\text{(energy solid)} \quad \nabla\left(k_s \nabla T_s\right) = 0$$

The computational domain is half of the microchannel width and half of the fin thickness, as depicted in Fig. 6, whereas the top lid is not included in the domain (Toh, 2002; Liu, 2005). A symmetry boundary condition is applied on both the outer vertical planes of the domain. At the inlet, a uniform velocity profile $u=u_i$ is imposed, whereas an average static pressure of zero is set at the outlet. A no-slip boundary condition is imposed along the internal channel surfaces. All the outer surfaces, apart from the bottom side where a uniform heat flux is applied, are treated as adiabatic in the solution of the energy equation. Continuity of both temperature and heat flux is specified at the solid-fluid interface. The solid material is aluminum with thermal conductivity $k_s=237$ *W/mK* and the cooling fluid is water with inlet temperature $T_i=298K$ and constant thermo-physical properties at a reference temperature of 300K ($k_s/k_f=409$). The governing equations along with the boundary conditions are solved on a structured grid, which consists of 902250 elements, using the commercial finite volume solver ANSYS CFX.

6.3 Numerical solution

None of the solutions that constitute the Pareto front is inferior to the others from the thermal and hydrodynamic performance point of view. Therefore, the final design point is chosen by considering additional aspects that concern the entire CPVT system, such as the total efficiency and the total cost of manufacturing. A FWμ heat sink with a channel width W_{ch} = 314 μm and a fin thickness of W_w = 169 μm is

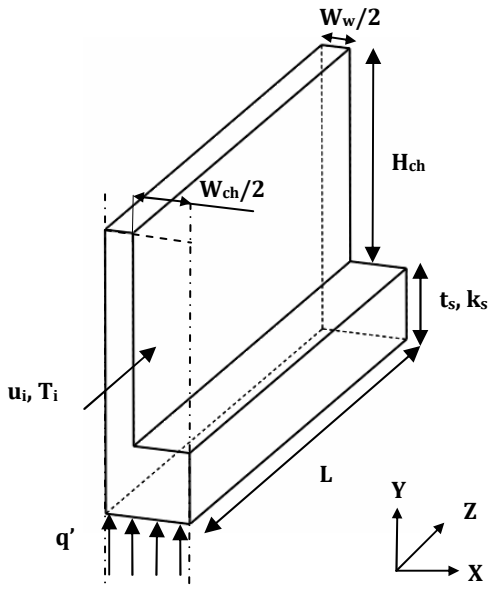

Fig. 6 Computational domain for the 3-D model.

Table 3
Comparison of the numerical values to the analytical ones.

					R_{th} (°C/W)		Δp (Pa)	
W_{ch} (μm)	W_w (μm)	H (μm)	Q (W/cm^2)	$\dot{V}_{tot}$ (mL/s)	Numerical	1-D model	Numerical	1-D model
314	169	1884	2.833	30.0	0.0090	0.0088	22809	21944

finally chosen as these geometric parameters apart from being a solution of the Pareto front, also correspond to very low parasitic (pumping) power and are easier to construct in comparison to the other optimal solutions due to the higher fin thickness. The substrate thickness t_s is chosen to be 1.5mm.

The total volumetric flow rate branches to 124 parallel channels of the heat sink and the Reynolds number that characterizes the flow inside each microchannel is 245 (inlet velocity of 0.409m/s). The computational domain is truncated to a total length L=0.09m approximately ten times the thermal entry length defined as:

$$L_{th} = L_{th}^{*} \,\mathrm{Re}\,\mathrm{Pr}\, D_h \qquad (17)$$

where $L_{th}^{*} \cong 0.011$ for a rectangular channel with $AR=6$ (Shah and Bhatti, 1987). This simplification is valid since the pressure distribution and the bulk fluid and bottom wall temperature distribution in the fully developed region vary linearly along the flow direction (Shah, 1978; Incropera, 1996).

The temperature contours on two cross-flow planes near the inlet and the outlet of the microchannel respectively, Fig. 7, illustrate that the channel bottom wall reaches its maximum temperature at the outlet, as expected. The bulk fluid and bottom wall temperature variation along the symmetry plane of the channel, illustrated in Fig. 8a, as derived from the 3-D model, exhibit clearly the linear trend in the fully developed region. Thus, it is justifiable to extrapolate the numerical values to a length of 0.5 m. The numerical values of the thermal resistance and the pressure drop were compared against the theoretically predicted ones and the results are presented in Table 3. A very good agreement is accomplished as the discrepancy in the values for the thermal resistance is 2.22% and for the pressure drop 3.79% respectively. Fig. 8b shows the variation of the local heat transfer coefficient in the thermally developing region, which exhibits a decaying trend towards an asymptotic value and Figs 8c-d depict the velocity and temperature distributions across the channel height in two positions along the flow direction. It is evident that the flow inside microchannels lays almost entirely in the fully developed region as both the fluid velocity and temperature rapidly obtain the corresponding profiles. It can be seen from Fig. 8c that the flow does not exhibit a parabolic but rather a characteristic flat velocity profile in the Y direction, which is in agreement with the theoretical profile. The velocity obtains instead the parabolic profile typical of fully-developed flow in the horizontal (XZ) plane of the microchannel. Referring to Fig. 8d, the development of the temperature profiles along the channel may be observed, with a clearly discernible linear part

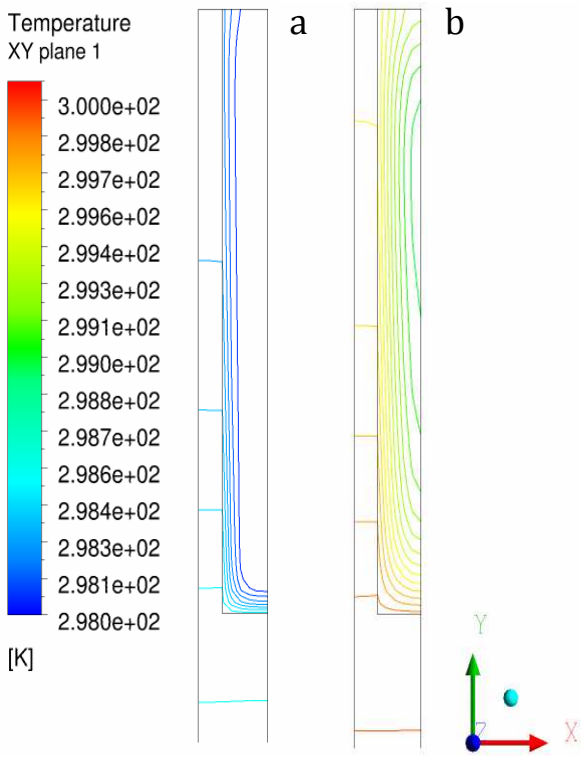

Fig. 7 Temperature contours on two planes, transversal to the flow: (a) Z=0.002m and (b) Z=0.088m.

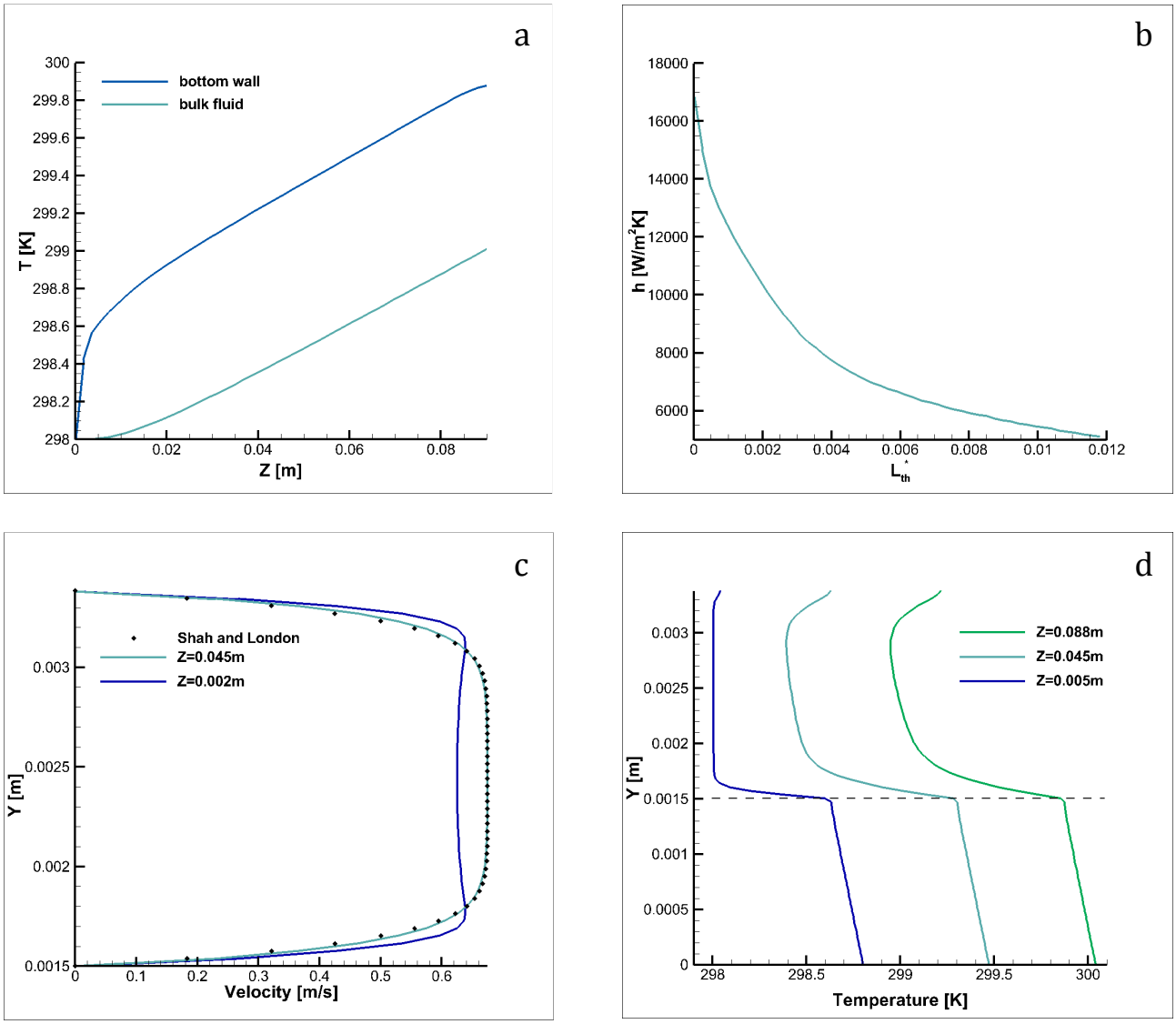

Fig. 8 Results on the central symmetry plane along the flow direction as obtained from the 3-D model: (a) bottom wall and bulk fluid temperature distributions, (b) local heat transfer coefficient in the developing region, (c) velocity profiles and (d) temperature profiles.

at the bottom, corresponding to the solid substrate. The increase in the fluid temperature in the vicinity of the top wall is due to the higher lateral heat flux in this region in connection with the reduced mass flux (reduced axial flow velocities) in the upper part of the microchannel.

7. Conclusions

In the present study, a multiobjective methodology was applied in order to optimize geometrical parameters of a microchannel heat sink suitable for a linear CPVT system. The optimized heat sink configurations exhibit enhanced thermal performance, while the introduction of stepwise variable-width microchannels significantly improves the hydrodynamic performance as well. Furthermore, by comparing the analytically predicted values to the 3-D numerical results, it has been proven that the 1-D analysis can fairly accurately represent the flow and conjugate heat transfer inside a microchannel, being therefore suitable for optimization procedure purposes.

Nomenclature

a	wall thickness to channel width ratio, *dimensionless*
A	area, m^2

AR	aspect ratio, *dimensionless*
c_p	specific heat, *J/kgK*
D_h	hydraulic diameter $D_h = \frac{2W_{ch}H_{ch}}{(W_{ch}+H_{ch})}$, *m*
f	Fanning friction factor, *dimensionless*
H	height, *m*
h	heat transfer coefficient $h = \frac{Nu \cdot k_f}{D_h}$, W/m^2K
k	thermal conductivity, *W/mK*
L	length, *m*
N	number, *dimensionless*
Nu	Nusselt number, *dimensionless*
p	pressure, *Pa*
P_{pump}	pumping power, *W*
Pr	Prandtl's number, *dimensionless*
Q	thermal power, *W*
q'	heat flux, W/m^2
R_{th}	thermal resistance, *K/W*
Re	Reynolds number, *dimensionless*
T	temperature, *K*
u	flow velocity, *m/s*
$\dot{V}$	volumetric flow rate, m^3/s
W	width, *m*

Greek symbols

μ	dynamic viscosity, $Pa \cdot s$
ν	kinematic viscosity, m^2/s
ρ	density, kg/m^3

Subscript

c	contraction
cal	caloric
conv	convective
cond	conductive
ch	channel
cs	cross section
d	developing
e	exit
f	fluid
fd	fully developed
hs	heat sink
i	inlet
init	initial
s	solid, section
th	thermal
tot	total
w	wall

References

Barrau, J., Chemisana, D., Rosell, J., Tadrist, L., Ibañez, M., 2010. An experimental study of a new hybrid jet impingement/micro-channel cooling scheme. Appl. Therm. Eng. 30, 2058-2066.

Blevins, R.D., 1984. Applied Fluid Dynamics Handbook, Van Nostrand Reinhold Company, New York.

Hilbert, R., Janiga, G., Baron, R., Thévenin, D., 2006. Multi-objective shape optimization of a heat exchanger using parallel genetic algorithms. Int. J. Heat Mass Transfer 49, 2567-2577.

Husain, A., Kim, K., Y., 2008. Shape optimization of micro-channel heat sink for micro-electronic cooling. IEEE Trans. Compon. Packaging Technol. 31, 322-330.

Incropera, F.P. and DeWitt, D.P., 1996. Fundamentals of Heat and Mass Transfer, Wiley, New York.

Jaluria, Y., 2009. Simulation-based optimization of thermal systems. Appl. Therm. Eng. 29, 1346–1355.

Knight, R.W., Goodling, J.S., Hall, D.J, 1991. Optimal thermal design of forced convection heat sinks-Analytical. J. Electron. Packaging 113, 313-321.

Kraus, A., Bar-Cohen, A., 1983. Thermal Analysis and Control of Electronic Equipment, McGraw-Hill, New York.

Lee, S., Qu, W., 2007. Thermal design methodology for low flow rate single phase and two-phase micro channel heat sinks. IEEE Trans. Compon. Packaging Technol. 30, 830-841.

Liu, D., Garimella S.V., 2005. Analysis and optimization of the thermal performance of microchannel heat sinks. Int. J. Num. Meth. Heat & Fluid Flow 15, 7-26.

Ndao, S., Peles, Y., Jensen, M.K., 2009. Multi-objective thermal design optimization and comparative analysis of electronics cooling technologies. Int. J. Heat Mass Transfer 52, 4317-4326.

Shah, R.K., Bhatti M.S., 1987. Chap. 3 in "Handbook of Single Phase Convective Heat Transfer", Kakac, S., Shah, R.K, Aung W., (editors), Wiley, New York.

Shah, R.K., 1978. A correlation for laminar hydrodynamic entry length solutions for circular and noncircular ducts. J. Fluids Eng. 100, 177-179.

Shah, R.K. and London A.L., 1978. Laminar Flow Forced Convection in Ducts: a Source Book for Compact Heat Exchanger, Academic press, New York.

The Mathworks Inc., 2004. Genetic Algorithm and Direct Search Toolbox for use with MATLAB, User's Guide, Version 1.

Toh, K.C., Chen, X.Y., Chai, J.C., 2002. Numerical computation of fluid flow and heat transfer in microchannels. Int. J. Heat Mass Transfer 45, 5133-5141

Tuckerman, D.B., Pease, R.F.W., 1981. High-performance heat sinking for VLSI. IEEE Electron. Device Letters 2, 126–129.